



## 저작자표시 2.0 대한민국

이용자는 아래의 조건을 따르는 경우에 한하여 자유롭게

- 이 저작물을 복제, 배포, 전송, 전시, 공연 및 방송할 수 있습니다.
- 이차적 저작물을 작성할 수 있습니다.
- 이 저작물을 영리 목적으로 이용할 수 있습니다.

다음과 같은 조건을 따라야 합니다:



저작자표시. 귀하는 원저작자를 표시하여야 합니다.

- 귀하는, 이 저작물의 재이용이나 배포의 경우, 이 저작물에 적용된 이용허락조건을 명확하게 나타내어야 합니다.
- 저작권자로부터 별도의 허가를 받으면 이러한 조건들은 적용되지 않습니다.

저작권법에 따른 이용자의 권리는 위의 내용에 의하여 영향을 받지 않습니다.

이것은 [이용허락규약\(Legal Code\)](#)을 이해하기 쉽게 요약한 것입니다.

[Disclaimer](#) 

공학석사 학위논문

**A Study on Electrical and Thermal Transportation  
properties of Nano-patterned CNT and Bismuth Film**

나노패턴이 삽입된 CNT와 Bismuth 박막의  
전기적, 열적 전달현상에 관한 연구

2012년 8월

서울대학교 대학원

재료공학부

정 승 우

**A Study on Electrical and Thermal Transportation  
properties of Nano-patterned CNT and Bismuth Film**

나노패턴이 삽입된 CNT와 Bismuth 박막의  
전기적, 열적 전달현상에 관한 연구

A DISSERTATION SUBMITTED TO  
SCHOOL OF MATERIALS SCIENCE AND ENGINEERING  
SEOUL NATIONAL UNIVERSITY

FOR THE DEGREE OF  
MASTER OF SCIENCE

Seungwoo Jung

August 2012

## **ABSTRACT**

Since it was revealed that nano-scale fabrication technique can enhance the thermoelectric properties of certain materials, nanomesh structure and nanowire has been applied to the materials which is potentially useful in thermoelectric devices. Those two strategies are applied to CNT film and Bismuth nanowire, respectively and electrical, thermal transport properties are investigated.

First, nanomesh pattern was inserted to CNT film and electrical, thermal, optical properties of the pristine CNT film and the nanomesh CNT film was investigated. Despite the small or near-zero Seebeck coefficient of metallic carbon nanotubes, a nanotube film can be readily scaled up in length. Thus so can its thermoelectric power. In this work, we inserted a nanomesh pattern into a carbon nanotube film by using an anodized aluminum oxide membrane as an etching mask. We found that by patterning densely packed nano-scale holes into the nanotube film, its total thermoelectric power can be further increased, by as much as 30% (from 29 to 39 V/K). We present this finding, attributed to electron localization due to nano-patterning, as indicative of the potential of a new degree of freedom.

Second, A Bismuth film with fine surface condition was fabricated with optimized deposition condition of PLD (Pulsed Laser Deposition)

system. The electrical properties and surface morphology of bismuth film by PLD was observed in the working pressure range from 10 mTorr to base pressure ( $10^{-6}$  Torr) and in the TS (target to substrate) distance range for 4cm ~ 7cm and temperature range from 22 °C to 200 °C. The electrical resistivity and surface morphology was varied with working pressure and TS distance and temperature. The bismuth film with 1.57 nm RMS surface roughness and around 300  $\mu\Omega\text{cm}$  value of electrical resistivity was deposited on a quartz substrate at optimized PLD deposition conditions. Eventually, bismuth nanowire was fabricated by e-beam lithography process and electrical property of the bismuth nanowire was investigated.

Keywords: Thermoelectric, nanomesh, AAO membrane, Seebeck coefficient, CNT film, Bismuth nanowire, Bismuth Hillock, Pulsed laser deposition

Student Number: 2010-22770

## TABLE OF CONTENTS

<b>ABSTRACT .....</b>	<b>i</b>
<b>TABLE OF CONTENTS.....</b>	<b>iii</b>
<b>LIST OF FIGURES .....</b>	<b>v</b>
<b>CHAPTER 1. Thermoelectric .....</b>	<b>1</b>
1. 1. Introduction .....	2
1. 2. Figure of merit .....	5
1. 3. Nano-scale strategies.....	8
1. 5. References .....	12
<b>CHAPTER 2. Nanomesh CNT film.....</b>	<b>13</b>
2.1. Introduction .....	14
2.2. Experiments.....	17
2.3. Results and discussion .....	20
2.4. Conclusion.....	26
2.5. References .....	27

<b>CHAPTER 3. Bismuth film and nanowire .....</b>	<b>29</b>
3.1. Introduction .....	30
3.2. Experiments.....	32
3.3. Results and discussion .....	34
3.6. References .....	45
<b>CHAPTER 4. Bismuth nanowire.....</b>	<b>46</b>
4.1. Experiments.....	47
4.2. Result and discussion .....	58
<b>Abstract (in Korean) .....</b>	<b>60</b>

# LIST OF FIGURES

## CHAPTER 1

**Figure 1-1.** Seebeck effect when two different metals exposed temperature gradient.

**Figure 1-2.** Schematic diagrams of thermoelectric power generator and cooler (heater) devices.

**Figure 1-3.** Room temperature ZT value development for past few decades [1].

**Figure 1-4.** Bi<sub>2</sub>Te<sub>3</sub>/Sb<sub>2</sub>Te<sub>3</sub> superlattice structure thin-film.

**Figure 1-5.** Nanomesh structure Si thin-film.

**Figure 1-6.** Corrugated and fine surface Si nanowires.



## CHAPTER 2

**Figure 2-1.** SEM images of (a) pristine CNT film and (b) nano-patterned CNT film. The scale bar is indicating 300 nm.

**Figure 2-2.** Thermovoltage of pristine CNT film and nano-patterned CNT film are measured at several temperature difference points. The slopes of this graph indicate TEPs of each pristine CNT film and nano-patterned CNT film. The TEP increased 33.6% in nano-patterned CNT film.

**Figure 2-3.** (a) Raman spectra and (b) UV/Vis/NIR absorption spectra of pristine CNT film and nano-patterned CNT film.

**Figure 2-4.** Temperature-dependent resistance of pristine CNT film and nano-patterned CNT film. Inset graph shows temperature-dependent resistance at low temperature region (80 K ~ 250K) and outset graph shows temperature-dependent resistance at high temperature region (250K ~ 330K).

## CHAPTER 3

**Figure 3-1.** Electrical property and surface morphology of bismuth thin-film by various physical vapor deposition methods are shown. All Cross-sectional SEM images and planar SEM images were taken with identical magnitude so those are having same scale bar.

**Figure 3-2.** Cross sectional SEM image of bismuth film with different working pressure for (a) No Ar gas, (b) Ar 1mtorr, (c) Ar 10mtorr. All scale bars indicate 100nm.

**Figure 3-3.** Cross sectional SEM image of bismuth film with different TS (target to substrate) distance for (a) 4cm, (b) 5cm, (c) 6cm and (d) 7cm. All scale bars indicate 100nm. The deposition rates are (a) 3.75 Å/sec (b) 2.8 Å/sec, (c) 2.41 Å/sec and (d) 1.24 Å/sec, respectively.

**Figure 3-4.** Cross sectional SEM image of bismuth film with different temperature for (a) 50 °C, (b) 100 °C, (c) 150 °C, (d) 200 °C. All scale bars indicate 1µm.

**Figure 3-5.** Change of the electrical resistivity as a function of deposition rate. Black dots indicate different working pressure, red dots indicate different TS distance, blue dots indicate different substrate temperature.

**Figure 3-6.**  $\theta - 2\theta$  XRD patterns of bismuth film deposited on glass

substrate by PLD with different deposition temperature (a), and  $\theta - 2\theta$  XRD patterns of bismuth film deposited in room temperature and its annealed sample with different annealing atmosphere (b). Both of the annealed samples have been placed in a quartz chamber in vacuum state for 6 hours.

**Figure 3-7.** AFM images of bismuth film by (a) thermal evaporator, (b) PLD and its annealed sample (c), RMS surface roughness values are (a) 24.2nm (b) 1.57nm (c) 1.29nm, respectively.

## CHAPTER 4

**Figure 4-1.** Schematic diagram of bismuth nanowire fabrication step

**Figure 4-2.** SEM images of bismuth nanowire fabricated by e-beam lithography process.

**Figure 4-3.** Optic image of electrodes deposited on bismuth nanowire.

**Figure 4-4.** SEM image of electrodes deposited on bismuth nanowire

**Figure 4-5.** Electrical property measurement of bismuth nanowire in various temperatures.

**Figure 4-6.** Electrical property measurement of bulk bismuth in various temperatures.

**Figure 4-7.** Temperature dependent electrical resistance of bismuth nanowire (a), bismuth thin film (b), bulk bismuth (c).

**Figure 4-8.** Temperature dependent electrical resistivity of bismuth nanowire, thin film and bulk.

**Figure 4-9.** Temperature dependent electrical resistivity of bismuth nanowire and thin film.

# CHAPTER 1.

## **Thermoelectric**

## 1. 1. Introduction

Approximately, 80% of energy consumption around the world is relying on fossil fuel combustion, and operates with 30~40% efficiency and generate a lots of dissipated heat. Because of this dissipated heat and by-products (like carbon oxide and carbon dioxide) from fossil fuel combustion, the global warming issue has been serious. Thermoelectric device is one of the promising techniques to relax this global warming problem, because it can transfer thermal energy to electrical energy and electrical energy to thermal energy. So, thermoelectric device can perform functions of energy harvesting and alternative energy source. The operating mechanism is based on Seebeck effect of materials. The Seebeck effect is the conversion on temperature gradients directly into voltage drop. The definition of Seebeck coefficient is  $S = -\frac{\Delta V}{\Delta T}$ , and in the figure 1-1 is the diagram of the circuit for measuring Seebeck coefficient. Sometimes, Seebeck coefficient is so called thermoelectric power. The Seebeck effect when two different metals placed on temperature gradient was indicated in figure 1-1. And the schematic diagrams of device for thermoelectric generator and thermoelectric cooler (heater) are indicated in figure 2-2.

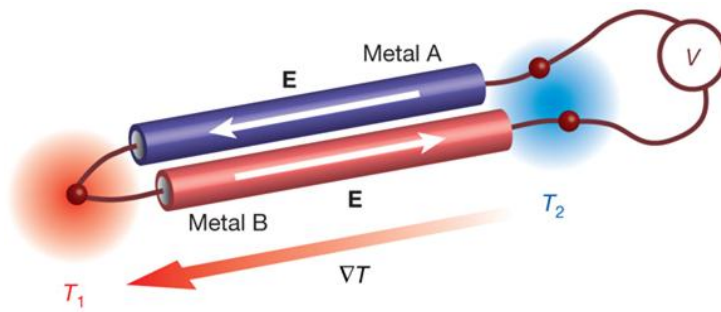


**Figure 1-1. Seebeck effect when two different metals exposed temperature gradient.**

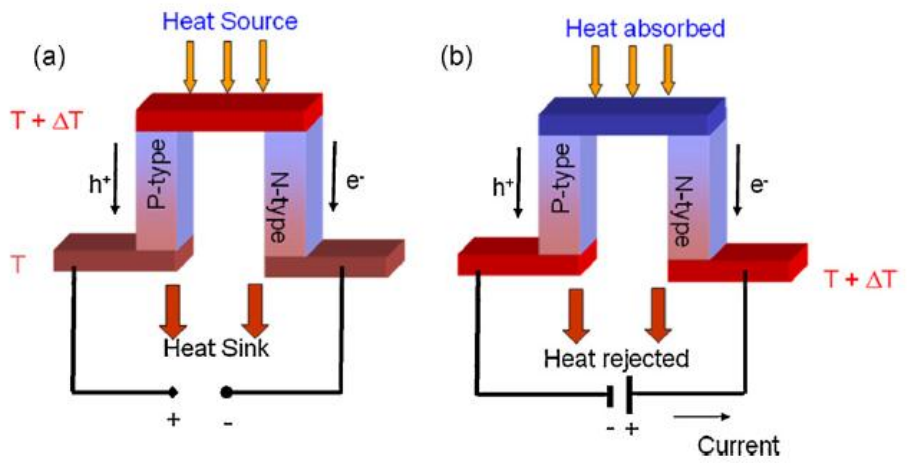


**Figure 1-2. Schematic diagrams of thermoelectric power generator and cooler (heater) devices.**



## 1. 2. Figure of merit

The efficiency of thermoelectric materials has been the critical barrier for commercialization of thermoelectric devices. The dimensionless figure of merit value is considered as efficiency of thermoelectric materials. The dimensionless figure of merit is so called ZT value and it is described as  $ZT = \frac{S^2\sigma}{\kappa}T$ . S is the Seebeck coefficient (Thermoelectric power),  $\sigma$  is the electrical conductivity,  $\kappa$  is the thermal conductivity and T is the average value of operating temperature defined as  $T = \frac{T_h+T_c}{2}$ . The ZT value of commercial thermoelectric cooler is around 1~2 in room temperature. And it is known that thermoelectric generator could be commercialized when room temperature ZT value reaches 3 and mass thermoelectric generator could be realized when room temperature ZT value exceeds more than 4 [1]. However increasing of ZT value is challenged because the Seebeck coefficient and electrical conductivity and thermal conductivity are strongly correlated each other and coupled through electrons and phonons in materials. Figure 1-3 shows the room temperature ZT value development for past few decades in the laboratory level. From late 1990s, ZT value has been increasing because nano-scale manipulation was introduced to thermoelectric

materials.

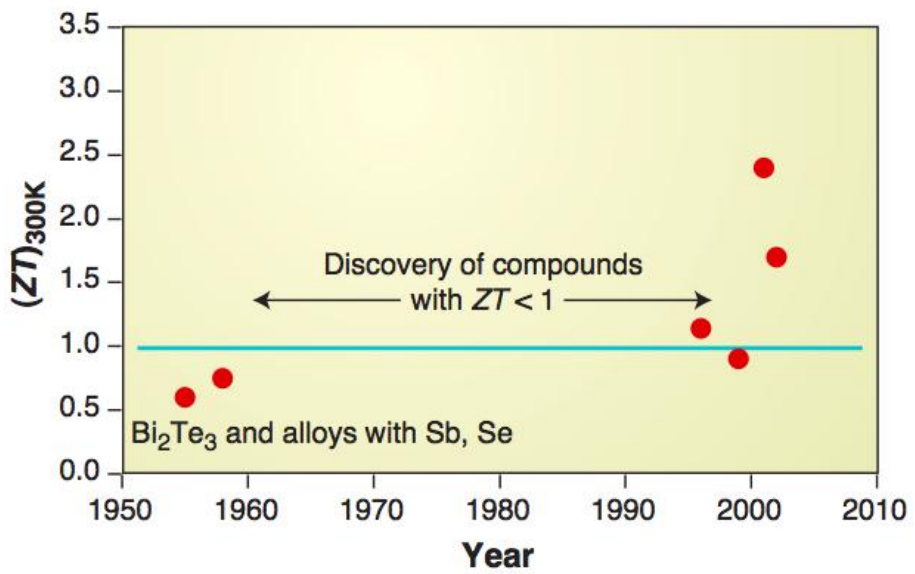


Figure 1-3. Room temperature ZT value development for past few decades [1].

### 1. 3. Nano-scale strategies

After nano-technology was widely researched, room temperature ZT value was further increased by electron-phonon decoupling. Actually, electrical conductivity and thermal conductivity in a material is strongly correlated to each other, which means if we want to increase one of them, the other should increase as much as the other one does. However, the ratio of electrical conductivity over thermal conductivity ( $\frac{\sigma}{\kappa}$ ) can be increased, if we use different nature of phonon and electron, then decouple these transporting to diminish thermal conductivity with not that much decreasing of electrical resistivity.

First, we can apply superlattice structure to vertical direction of thin-films. In this structure, phonon propagation along cross-plane direction is diminished, because phonon is atomic vibration and it is exposed to different atomic mass. but electron propagation is not that decreased, because lattice mismatch is almost negligible [2]. Figure 1-4 shows the  $\text{Bi}_2\text{Te}_3/\text{Sb}_2\text{Te}_3$  superlattice structure thin-film.

Second, we can apply nanomesh or corrugated structure of nanowire, normally mean free path of electron is much smaller than mean free path of phonon. so if the feature size of material is between two MFP scale, thermal conductivity can be diminished with not that

decreasing of electrical conductivity [3,4]. Figure 1-5 and 1-6 shows Si nanomesh structure and corrugated Si nanowire.

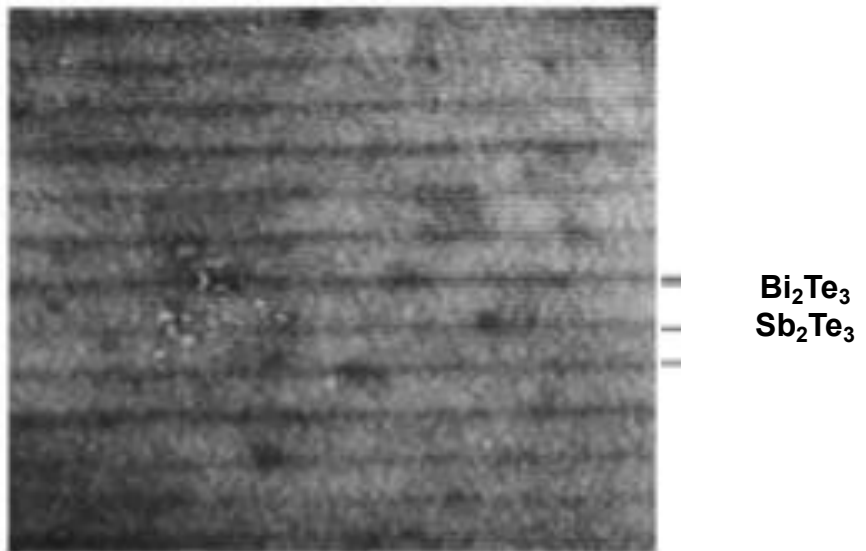


**Figure 1-4. Bi<sub>2</sub>Te<sub>3</sub>/Sb<sub>2</sub>Te<sub>3</sub> superlattice structure thin-film.**

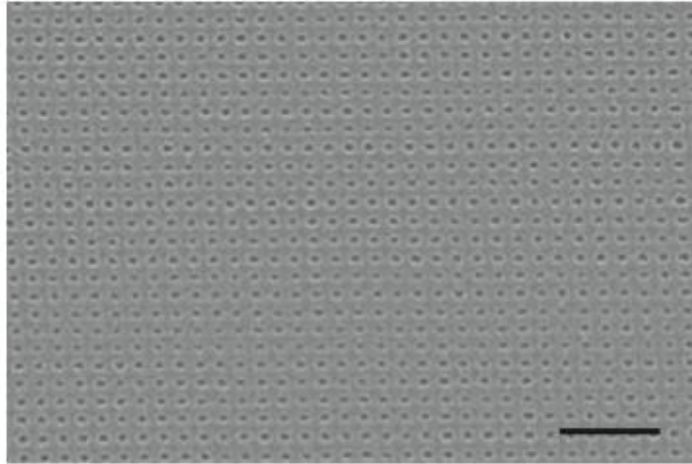


**Figure 1-5. Nanomesh structure Si thin-film.**

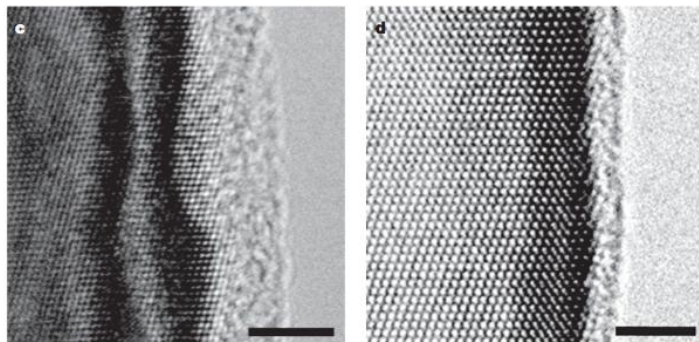


**Figure 1-6. Corrugated and fine surface Si nanowires.**

## 1. 5. References

- [1] Majumdar A 2004 *Science* **303** 5659
- [2] Venkatasubramanian R, Siivola E, Colpitts T and O' Quinn B 2001 *Nature* **413** 6856
- [3] Yu J-K, Mitrovic S, Tham D, Varghese J, and Heath J R 2010 *Nat. Nanotechnol.* **5** 718
- [4] Hochbaum A I, Chen R, Delgado R D, Liang W, Garnett E C, Najarian M, Majumdar A and Yang P 2008 *Nature* **451** 163



## CHAPTER 2.

### **Nanomesh CNT film**

## 2.1. Introduction

Carbon nanotube films are generally not considered as a leading contender for thermoelectric energy harvesting, largely because the metallic nanotubes exhibit a zero or near-zero Seebeck coefficient and because the conductivity of a random network of nanotubes is dominated by the metallic ones. On the other hand, a nanotube film can readily be scaled up in length, along with its total thermoelectric power to a sizable value even with just a small Seebeck coefficient.

A random network of carbon nanotubes (CNTs) is an interesting system for basic sciences and engineering [1, 2]. Many interesting questions remain open or underexplored, one of which is its thermoelectricity [3, 4]. A pristine metallic nanotube is expected to exhibit no thermoelectric power (TEP), yet experiments showed otherwise [4]. Theoretical expectation on TEP of a CNT film is also intriguing but more complex because the coupling between tubes and spatial charge transfer between tubes are involved. Maximizing the power and efficiency of the thermoelectric (TE) device is the key issues of its commercialization [5]. The power factor of a TE device is expressed as  $S^2\sigma$  and the efficiency of TE material is defined as  $ZT = \frac{S^2\sigma}{K}T$ . Here,  $ZT$  is a dimensionless figure of merit,  $S$  is the

TEP (Seebeck coefficient),  $\sigma$  is the electrical conductivity,  $K$  is the thermal conductivity and  $T$  is the absolute temperature [6]. Nanopatterning has been proposed as one strategy for increasing  $ZT$  [7, 8]. If the feature size imposed on the material is between the phonon mean free path and electron mean free path, the transport of electron could be decoupled from that of phonon so as to substantially reduce the thermal conductivity without considerably affecting the electrical conductivity. This strategy is preferable in semiconducting materials than in metallic materials because much of the thermal-transport in metallic materials is done by electrons while in semiconducting materials phonons contribute more to the thermal conductance. However, a carbon nanotube film is not simply metallic or semiconducting material. The electrical properties of a CNT film depend on the chirality of the CNTs and on carrier hopping between CNT strands which occurs with certain activation energy [9, 10]. In order to study the effect of electron-phonon decoupling in CNT films in terms of TE properties, a CNT nanomesh film was fabricated. It is a non-trivial task to measure Seebeck coefficient in nano-scale dimension samples because temperature drop through a material is not easy to be developed if the two ends are too close. Here, we made CNT nanomesh film by reactive ion etch (RIE) using anodized aluminum oxide (AAO) as etching mask. Because of

the scalability of AAO fabrication, the sample can be fabricated with relatively large dimension (a few cm<sup>2</sup>), which can help the Seebeck coefficient measurement of the sample and fabrication of large area TE device using CNT. In this work, we studied two types of CNT films, one subjected to nano-patterning and the other not. In the nano-patterned CNT film, a substantial increase, up to 30%, in TEP was measured.

## 2.2. Experiments

A surfactant-dispersed single-walled CNT solution (1% sodium dodecyl sulfate), which is composed of 1/3 semiconducting CNT and 2/3 metallic CNT, average diameter around 1.4nm, was purchased from Nanointegris, Inc. The main motivation of using this specific composition (1/3 semiconducting and 2/3 metallic) is based firstly on this being the commonly obtained yield in most CNT synthesis processes and secondly we found that purely semiconducting and purely metallic SWCNT films exhibited slightly lower TEP at room temperature during our initial investigation. Thin films of CNTs on glass substrate were prepared by membrane filtration method [11] and the obtained thickness was 20 nm. Nano-patterning was carried out by RIE, in which AAO was used as etch mask. The fabrication method of the AAO membrane is discussed by Chik et al [12]. After AAO membrane fabrication, the AAO pores were widened to ~50 nm diameter in a 0.5M phosphoric acid ( $H_3PO_4$ ) solution at 33 °C. The AAO membrane was then detached from the aluminum substrate by using mercuric chloride ( $HgCl_2$ ), and the barrier oxide layer was removed by treating it with phosphoric acid ( $H_3PO_4$ ) for 10 minutes at room temperature (22 °C). The floating AAO membrane on DI water was transferred to the CNT film and RIE was performed with a gaseous mixture of HCl at 5 sccm, Cl at

30 sccm, 50 mTorr of working pressure, 100 W of RF power, and 5 minutes of etch time. For future applications, we note both of CNT film and AAO are scalable in size. The nano-pattern has 100 nm period and 50 nm pores. The SEM image of pristine CNT and nano-patterned CNT films are shown in Figure 2-1. The sheet resistance was measured by a typical four-probe setup, UV/Vis/NIR spectra (Cary 500, Varian) and Raman spectra were obtained for both pristine and nano-patterned CNT samples. In order to measure TEP (Seebeck coefficient), the sample was located between thermoelectric cooling block (cold end) and resistive heating block (hot end) to create temperature difference between two ends. The temperatures of two ends were measured by micro-tip thermocouple with a small amount of thermal paste applied to the tip of the thermocouple to improve thermal contact. The TE voltage was measured across two ends by thin copper-wire electrodes. The temperature dependent electrical resistance was measured in a cryostat at  $\sim 10^{-3}$  Torr. The sample was first cooled by liquid nitrogen and measurements were taken at various temperatures in 5 K intervals as the sample temperature was increased with a heater mounted in the cold finger of the cryostat.

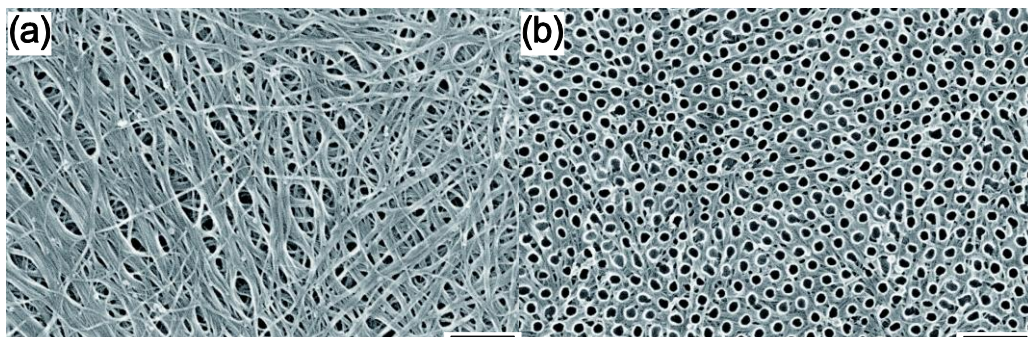


**Figure 2-1. SEM images of (a) pristine CNT film and (b) nano-patterned CNT film. The scale bar is indicating 300 nm.**

## 2.3. Results and discussion

Figure 2-2 shows TEPs of pristine CNT and nano-patterned (nanomesh) CNT films. The linear slopes of the measured points indicate the TEP for each sample. The TEP of pristine CNT film and nanomesh CNT film is  $29.54 (\pm 1.2) \mu\text{V/K}$  and  $39.47 (\pm 0.7) \mu\text{V/K}$ , respectively. The TEP increased 33.6% in nanomesh CNT structure, and the value of pristine CNT film is well matched to previously reported data [13]. The sheet resistance of pristine CNT film was  $0.8 (\pm 6.5\%) \text{ m}\Omega/\text{sq.}$  and the nano-patterned CNT film was  $16.4 (\pm 8.6\%) \text{ m}\Omega/\text{sq.}$ . After accounting for the volume filling factor calculated by a MATLAB software image analysis routine, 97.77% for pristine CNT film and 77.49% for nanomesh CNT film, it turned out that electrical resistivity was 16 times larger in the nanomesh CNT film compared with the pristine film. Nanohole scattering and damaged  $sp^2$  bonds can both affect the sheet resistance. The Raman G to D peak ratio of pristine CNT film was found to be around 39 and only 14 for the nano-patterned CNT film, as shown in the Raman spectra in Figure 2-3 (a).

Figure 2-3 (b) shows UV/Vis/NIR spectra of the pristine and nano-patterned CNT films. Several peaks around 400~600 nm are from the S33 transition and the peak around 1050 nm corresponds to the S22 transition in semiconducting CNTs. The peak between 650~750 nm corresponds to the M11 transition in metallic CNTs [14]. In nano-patterned CNT film, peak areas of these transitions were decreased, because of broken  $sp^2$  bond. The S22



transition peak is slightly blue shifted by 0.05 eV in nano-patterned CNT film.

Figure 2-4 shows the temperature-dependent electrical resistance of pristine and nanomesh CNT films. The linear slopes of this graph indicate energy barriers for variable range hopping (VRH) conduction [9, 10]. The temperature-dependent resistance described by VRH is

$$R(T) = R_0 \exp[-(T_0/T)^a] \quad (1)$$

Where  $R_0$  is a constant,  $T_0$  is the temperature necessary for thermal fluctuations to overcome the tunneling barrier between the nanotubes and  $a$  is the dimensionality of hopping in Mott's VRH model. The  $a$  is 1/2 for one-dimensional transport and 1/4 for three-dimensional transport [15].

$$\frac{R(T)}{R(300K)} = \frac{R_0 \exp[-(T_0/T)^a]}{R_0 \exp[-(T_0/300K)^a]}$$

$$\ln\left(\frac{R(T)}{R(300K)}\right) = \left(-\frac{T_0}{T}\right)^a + \left(\frac{T_0}{300K}\right)^a \quad (2)$$

In Eq. (2),  $T_0$  can be obtained from a plot of  $\ln[R(T)/R(300K)]$  versus  $T^{-a}$  using linear regression. It was reported that electronic transport within the intrinsic SWCNT network is determined by the three-dimensional electron hopping mechanism [9]. Therefore, 1/4 is used for the value of  $a$  in this plot. The inset graph of figure 2-4 shows the temperature-dependent electrical resistivity in the range of 250 K ~ 80 K. Below 250 K, the energy barriers of the pristine CNT film and the nanomesh CNT film are 1.15 meV (13.4 K) and 39.3 meV (456 K), respectively. Above 250 K, the pristine CNT film behaves

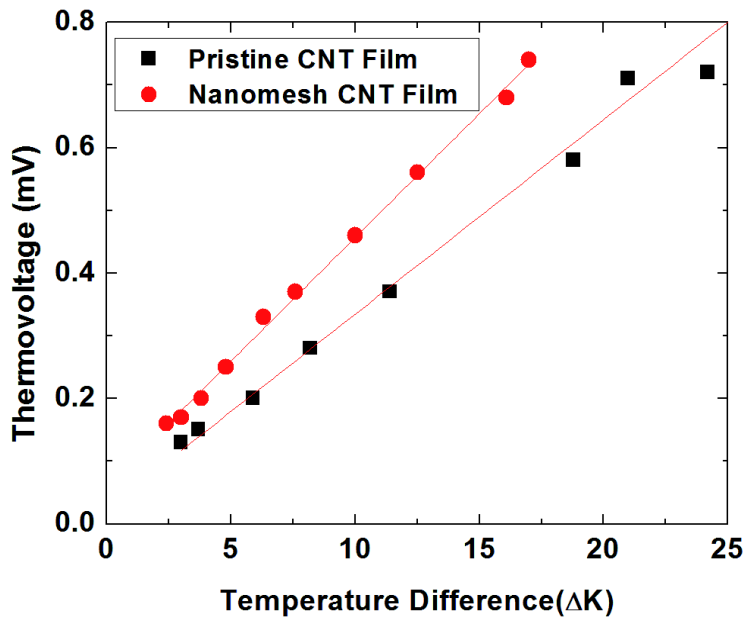


**Figure 2-2.** Thermovoltage of pristine CNT film and nano-patterned CNT film are measured at several temperature difference points. The slopes of this graph indicate TEPs of each pristine CNT film and nano-patterned CNT film. The TEP increased 33.6% in nano-patterned CNT film.

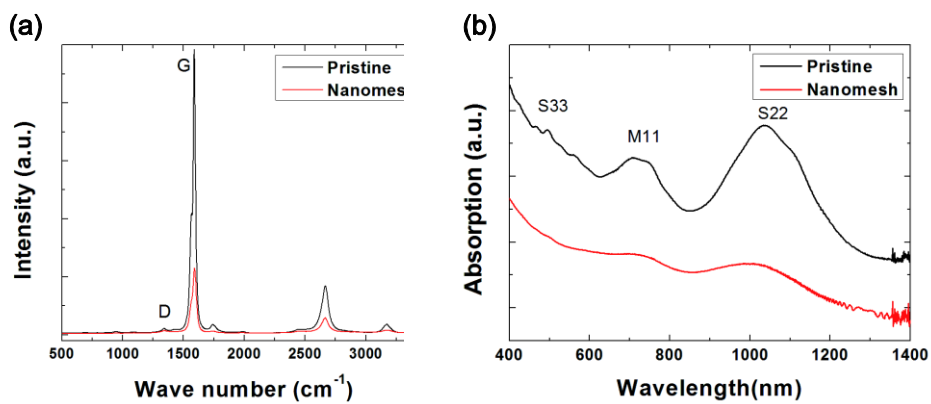


**Figure 2-3. . (a) Raman spectra and (b) UV/Vis/NIR absorption spectra of pristine CNT film and nano-patterned CNT film.**

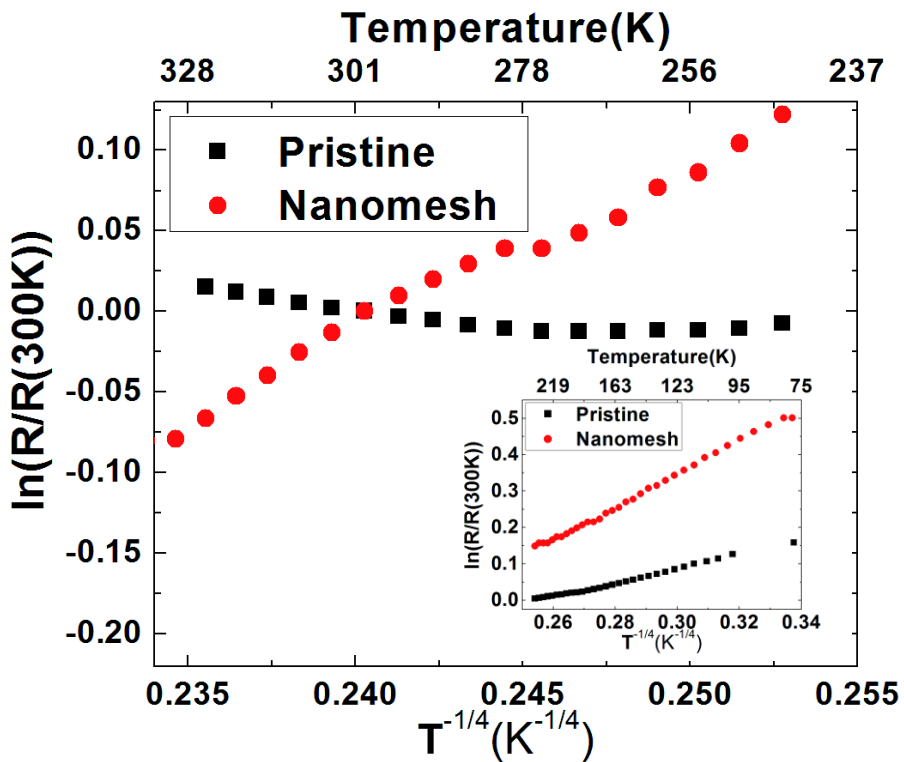


Figure 2-4. Temperature-dependent resistance of pristine CNT film and nano-patterned CNT film. Inset graph shows temperature-dependent resistance at low temperature region (80 K ~ 250K) and outset graph shows temperature-dependent resistance at high temperature region (250K ~ 330K).

like a metal with positive temperature coefficient of resistance (TCR) and the nanomesh CNT film show much higher energy barrier ( $0.95 \text{ eV} = 11,074 \text{ K}$ ) than below 250 K. The TCR value of the pristine CNT film and the nanomesh CNT film is  $0.04 \text{ \%}/\text{K}$  and  $-0.2 \text{ \%}/\text{K}$  respectively. It is remarkable that the TCR value increased by 5 times in the nanomesh structure. The temperature dependent resistivity of pristine CNT film agrees well with previous data [16]. The thermal assisted electron hopping from a CNT to another is saturated around 250 K when the pristine CNT film became metallic. In an isolated metallic nanotube, a zero or near zero Seebeck coefficient is expected of the symmetric conduction and valence bands around the Fermi level. A rich concentration of metallic nanotubes in the film suggests that the film conductivity is dominated by metallic tubes. The measured small but finite Seebeck coefficient in the pristine nanotube film indicates that spatial charge transfer between tubes and between metallic tubes and semiconducting ones played a role, one that is equivalent to doping. The nano-patterning contributed further to the equivalent doping through the  $sp^2$  to  $sp^3$  bond conversion at the defect sites and through oxygen termination of the broken bonds, both of which have the effect of localizing (i.e. doping) some of the otherwise mobile pi electrons. The substantial increase in Seebeck coefficient and the semiconducting behavior persisted beyond 250 K in the nanopatterned CNT film may therefore be understood in terms of these electron localization effects [17].

## 2.4. Conclusion

In our experiment, we have compared the TEP, electrical and optical properties between pristine and nanomesh CNT films. Compared to the pristine CNT film, the nanomesh CNT film showed a 33.6% increase in the TEP and a 5-fold increase in the TCR. For thermoelectric energy harvesting, the 33.6% increase in TEP alone is not sufficient. A decrease in thermal conductance, greater than the decreased electrical conductivity, would also be required, which seems possible with further nano-pattern designs targeting specifically the phonon transport. This will lead us to the conclusion that the thermoelectric property of the nanopatterned CNT film might be improved by controlling the size of pores and geometric shape. Moreover, the electrical conductivity of the nanopatterned CNT film might be improved by chemical treatment or annealing, or doping of the CNTs.

## 2.5. References

- [1] Snow E S, Novak J P, Campbell P M and Park D 2003 *Appl. Phys. Lett.* **82** 2145
- [2] Suhr J and Koratkar N A 2008 *J. Mater. Sci.* **43** 4370
- [3] Hewitt C A, Kaiser A B, Roth S, Craps M, Czerw R and Carroll D L 2011 *Appl. Phys. Lett.* **98** 183110
- [4] Hone J, Ellwood I, Muno M, Mizel A, Cohen M L, Zettl A, Rinzler A G and Smalley R E 1998 *Phys. Rev. Lett.* **80** 1042
- [5] DiSalvo F J 1999 *Science* **285** 703
- [6] Venkatasubramanian R, Siivola E, Colpitts T and O`Quinn B 2001 *Nature* **413** 597
- [7] Yu J-K, Mitrovic S, Tham D, Varghese J, and Heath J R 2010 *Nat. Nanotechnol.* **5** 718
- [8] Hochbaum A I, Chen R, Delgado R D, Liang W, Garnett E C, Najarian M, Majumdar A and Yang P 2008 *Nature* **451** 163
- [9] Han Z J and Ostrikov K 2010 *Appl. Phys. Lett.* **96** 233115
- [10] Skákalová V, Kaiser A B, Woo Y-S and Roth S 2006 *Phys. Rev. B* **74** 085403
- [11] Wu Z, Chen Z, Du X, Logan J M, Sippel J, Nikolou M, Kamaras K, Reynolds J R, Tanner D B, Hebard A F and Rinzler A G 2004 *Science* **305** 1273

- [12] Chik H and Xu J M 2004 *Mater. Sci. Eng. R Rep.* **43** 103
- [13] Romero H E, Sumanasekera G U, Mahan G D and Eklund P C 2002 *Phys. Rev. B* **65** 205410
- [14] Itkis M E, Perea D E, Jung R, Niyogi S and Haddon R C 2005 *J. Am. Chem. Soc.* **127** 3439
- [15] Peng H 2008 *J. Am. Chem. Soc.* **130** 42
- [16] Itkis M E, Borondics F, Yu A and Haddon R C 2006 *Science* **312** 413
- [17] Goldsmid H J and Sharp J W 1999 *J. Electron. Mater.* **28** 869



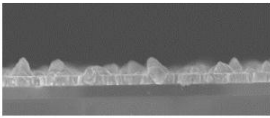
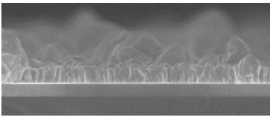
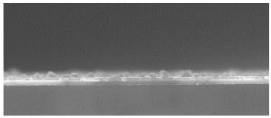
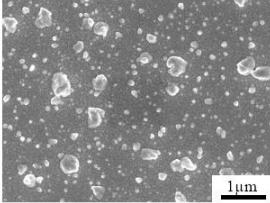
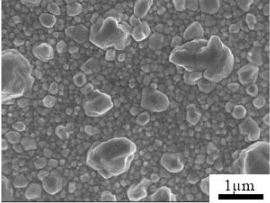
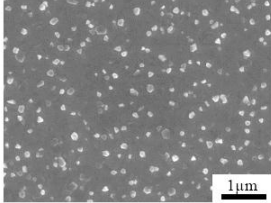
## CHAPTER 3.

### **Bismuth film and nanowire**

### 3.1. Introduction

The serious anxiety about extinction of fossil fuel source and global warming associated with fossil fuel sources has stimulated the research for sustainable and clean energy sources. Among the various alternative energy sources and technologies, thermoelectricity (TE) device has been received a lots of attention because it can convert thermal energy to electrical energy and vice versa [1]. However, maximum power and efficiency of a TE device is the key issues of its commercialization. The efficiency of TE material is defined as :  $\frac{S^2\sigma}{\kappa}T$ . Here, ZT is called dimension less figure of merit and S is Seebeck coefficient,  $\sigma$  is electrical conductivity,  $\kappa$  is thermal conductivity, T is absolute temperature [2]. Bismuth is group V semi-metallic element and having lowest thermal conductivity among metallic elements and bismuth exhibits abnormal transport behavior due to its highly anisotropic Fermi surface [3,4]. Because of that, bismuth has been issued in nanophysics field by both of experimentalists and theorists. Also, it is theoretically addressed that nano-fabrication of bismuth will increase the ZT value of bismuth film [5]. The hillocks on bismuth thin film surface formed during deposition was discovered, however, it obstructs further fabrication step to make 1D nanowire by e-beam

lithography and also application for micro-chips and IC industries [6,7]. There are several reports about deposition of bismuth film by using sputter [6], thermal evaporation [7] and pulsed laser deposition (PLD) [8]. The results of our preliminary deposition test are indicated in figure 3-1. We have seen some opportunities that surface roughness of bismuth film can be reduced with appropriate PLD deposition condition. In order to remove the hillocks that cause high surface roughness, and reduce electrical resistivity of bismuth thin film, deposition condition of pulsed laser deposition (PLD) system was varied in terms of working pressure, TS (target to substrate) distance, temperature.

	DC Sputtering	RF Sputtering	Thermal evaporation
SEM Image			
			
Resistivity	1350 $\mu\Omega\text{cm}$	1065 $\mu\Omega\text{cm}$	395 $\mu\Omega\text{cm}$
Thickness	250 nm	300 nm	80nm
Deposition Rate	7 $\text{\AA}/\text{sec}$	8.3 $\text{\AA}/\text{sec}$	50 $\text{\AA}/\text{sec}$
TS Distance	4.5 cm	4.5 cm	25 cm

**Figure 3-1. Electrical property and surface morphology of bismuth thin-film by various physical vapor deposition methods are shown. All Cross-sectional SEM images and planar SEM images were taken with identical magnitude so those are having same scale bar.**

### 3.2. Experiments

Bismuth films were deposited on quartz substrates by home-made laser ablation system using Nd:YAG (Neodymium-doped Yttrium Aluminum Garnet;  $\text{Nd:Y}_3\text{Al}_5\text{O}_{12}$ ) for laser source, laser power and repetition rate was 150mW and 5Hz, respectively. Energy density was fixed to  $1.5\text{J}/\text{cm}^2$ . Bismuth target (99.999%, LTS research laboratory, INC., New York) was keep rotating during the deposition. Three controllable parameters were changed during this experiment. The working pressure (Ar gas) was changed for 10 mTorr, 1 mTorr and no Ar gas ( $10^{-6}$ Torr), TS (target to substrate) distance for 4 cm, 5 cm, 6 cm, 7 cm without any inert gas incoming, substrate temperature for 50 °C, 100 °C, 150 °C, 200 °C. Surface morphology was analyzed by cross sectional scanning electron microscopy (SEM, JEOL JSM-7401F) image, and electrical resistivity was measured by conventional 4-point probe method. Crystal orientation of the bismuth films were observed by X-ray diffraction patterns (New D8 advance, Bruker) in the conventional  $\theta - 2\theta$  mode and RMS surface roughness was measured by non-contact mode atomic force microscopy (AFM, Seiko SPA-400) system.

### 3.3. Results and discussion

The cross sectional SEM images of bismuth film in different working pressure are shown in figure 3-2. The roughness of bismuth film is getting higher as working pressure is increased and all films were deposited on room temperature. Relatively fine surface was deposited when Ar gas is not injected into the chamber. This tendency is similar to the previously reported result. [9] Figure 3-2 shows cross sectional SEM images of bismuth film deposited without Ar gas, in different TS distance at room temperature. The TS distance and deposition time for figure 3-3 (a) is 4cm, 8min, (b) is 5cm, 9min, (c) is 6cm, 10min and (d) is 7cm, 11min. As in SEM images, the surface roughness is not significantly changed with TS distance but, deposition rate is increasing with TS distance decreasing. Figure. 3-4 shows cross sectional SEM images of bismuth film in different substrate temperature, in the condition without Ar gas and TS distance for 4cm. In 100 °C, 150 °C, rough films have deposited with hillock structure and in 200 °C, bismuth has agglomerated and the film is not continuous. However, In 50 °C hillock-free fine surface of bismuth film was obtained. Surface morphology is related with diffusion length during deposition.

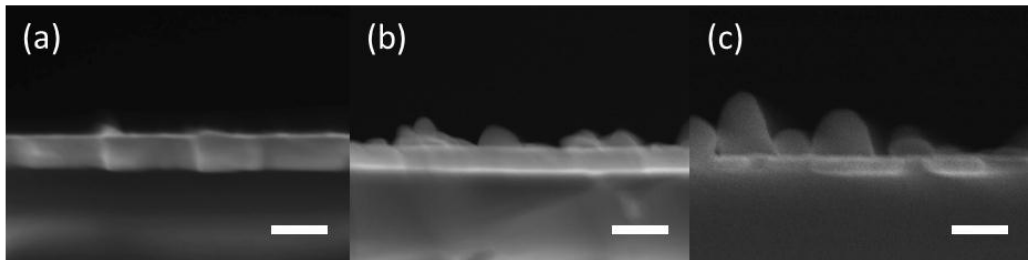


**Figure 3-2 Cross sectional SEM image of bismuth film with different working pressure for (a) No Ar gas, (b) Ar 1mtorr, (c) Ar 10mtorr. All scale bars indicate 100nm.**

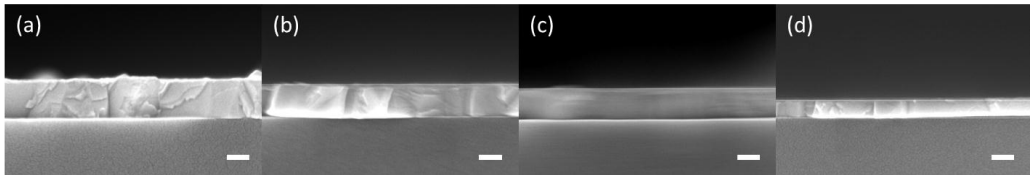


**Figure 3-3. Cross sectional SEM image of bismuth film with different TS (target to substrate) distance for (a) 4cm, (b) 5cm, (c) 6cm and (d) 7cm. All scale bars indicate 100nm. The deposition rates are (a) 3.75 Å/sec (b) 2.8 Å/sec, (c) 2.41 Å/sec and (d) 1.24 Å/sec, respectively.**



Diffusion length (L) is expressed as,

$$L = \sqrt{2Dt} = \sqrt{2D_0 \exp\left(-\frac{E_a}{k_B T}\right) t} .$$

It is observed that bismuth plume shape is getting broad with increasing working pressure. So, lower working pressure makes bismuth plume shape more linear then increase deposition rate. These factors cause the reducing interval time of bismuth atoms (molecules) arrival and diffusion lengths were decreased and hillocks cannot be made. Deposition rate was also changed with TS distance but, surface morphology was not changed with TS distance, even hillocks are not formed in 7 cm TS distance. The kinetic energy of sputtered bismuth atom or molecule is losing at scattering events along TS distance when Ar gas exists. However the kinetic energy would not significantly decrease enough to form hillock when Ar gas is absent in the chamber. This would be a reason for not forming hillocks at 7 cm TS distance when Ar gas is not injected to the chamber. Surface roughness is increasing with temperature. It is not certain whether because of diffusion length effect or agglomeration effect, as figure. 3-4 (b), (c) shows both of morphologies and agglomerated film on figure 3-4 (d). In the figure 3-5, electrical resistivity is plotted as a function of variable deposition conditions and deposition rate. Black dot is for different working pressure and red dot is for different TS distance and blue dot is

for different substrate temperature. This figure is showing that low electrical resistivity is obtained at low working pressure and short TS distance, since deposition rate is related with working pressure and TS distance. High deposition rate can reduce oxidation probability and hillocks on bismuth surface which enhance surface scattering effect of electrons, compared the declining slopes of red dots and black dots in figure 3-5 (b). The electrical resistivity is related with temperature, as well. It decreased up to 100 °C, and increases at 150 °C again. Annealing effect and oxidation probability can affect the electrical resistivity change with temperature, there is a tendency that electrical resistivity is inversely proportional to deposition rate.

In the figure 3-6 (a), X-ray diffraction patterns for bismuth film by PLD system with different deposition temperature are indicated. For the bismuth films deposited in 150°C and 100°C, peaks of different crystal plane, i.e. (012), (104), (110), (015), and (017), indicates that the film is polycrystalline with random orientation. However, the bismuth films deposited in 50°C and room temperature have highly oriented crystal structure with strongly preferred at (003) direction. Figure 3-6 (b) shows XRD patterns of annealed sample with different atmosphere and its pristine film (deposited in room temperature). Bismuth oxide peak

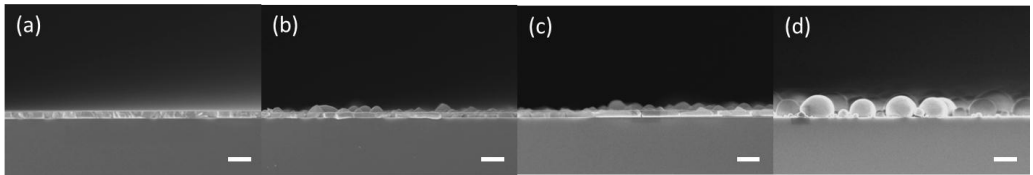


**Figure 3-4. Cross sectional SEM image of bismuth film with different temperature for (a) 50 °C, (b) 100 °C, (c) 150 °C, (d) 200 °C. All scale bars indicate 1 $\mu$ m.**

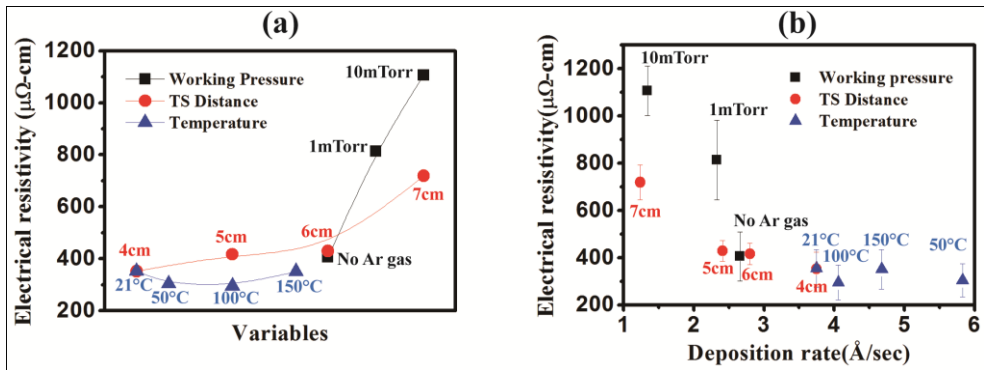


**Figure 3-5. Change of the electrical resistivity as a function of deposition rate. Black dots indicate different working pressure, red dots indicate different TS distance, blue dots indicate different substrate temperature.**

was appeared with Ar atmosphere. However, the peak is not appeared with Ar and H<sub>2</sub> atmosphere. The bismuth peak was appeared in Ar atmosphere because oxygen gas was not completely removed in the annealing chamber. The oxidation probability was lowered by flow hydrogen gas so that takes oxygen away. The peak intensity of bismuth crystal plane i.e. (003), (006), (009), was increased by annealing process which is performed at 250 °C for 6 hours in the atmosphere of Ar and H<sub>2</sub>. The electrical resistivity is not changed after annealing process.

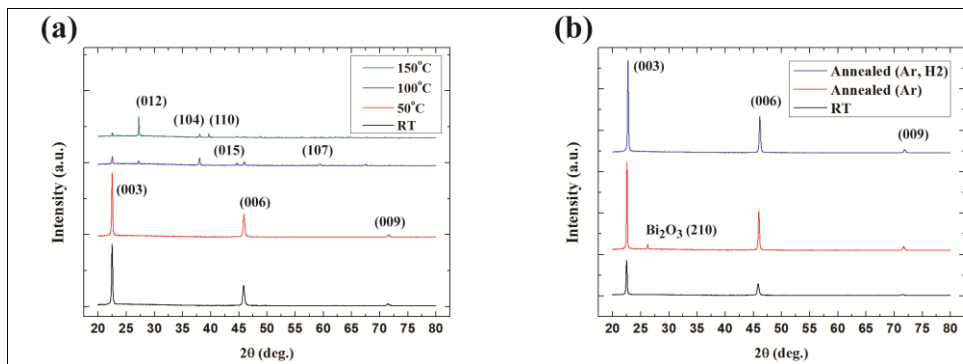


**Figure 3-6.  $\theta$  -  $2\theta$  XRD patterns of bismuth film deposited on glass substrate by PLD with different deposition temperature (a), and  $\theta$  -  $2\theta$  XRD patterns of bismuth film deposited in room temperature and its annealed sample with different annealing atmosphere (b). Both of the annealed samples have been placed in a quartz chamber in vacuum state for 6 hours.**

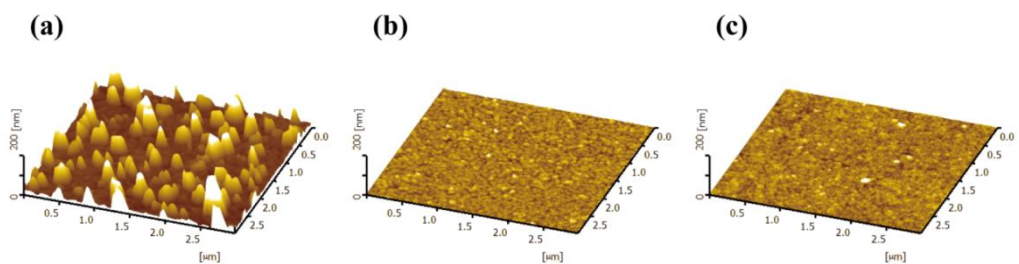


**Figure 3-7. AFM images of bismuth film by (a) thermal evaporator, (b) PLD and its annealed sample (c), RMS surface roughness values are (a) 24.2nm (b) 1.57nm (c) 1.29nm, respectively.**

In the figure 3-7, the topological images of the bismuth films are

indicated as AFM image. The AFM image of the bismuth film deposited by thermal evaporator is shown in figure 3-7 (a). There are obviously hillocks on the surface, average height with around 70nm and RMS surface roughness value is 24.2nm. Those hillocks were not appeared in the optimized PLD deposition condition and it can be proved with AFM images shown in figure 3-7 (b). Even, the hillocks are not formed after annealing which is performed at 250 °C for 6 hours in the atmosphere of Ar and H<sub>2</sub>.



### 3.6. References

- [1] DiSalvo F J 1999 *Science* **285** 703
- [2] Venkatasubramanian R, Siivola E, Colpitts T and O' Quinn B 2001 *Nature* **413** 6856
- [3] Heremans J, Thrush C, Lin Y, Cronin S, Zhang Z, Dresselhaus M S and Mansfield J F 2000 *Phys. Rev. B* **61** 2921
- [4] Zhang Z, Sun X, Dresselhaus M S, Ying J and Heremans J 2000 *Phys. Rev. B* **61** 4850
- [5] Hicks L D and Dresselhaus M S 1993 *Phys. Rev. B* **47** 16631
- [6] Kim D H, Lee S H, Kim J K and Lee G H 2006 *Appl. Surf. Sci.* **252** 3525
- [7] Rogacheva E I, Grigorov S N, Nashchekina O N, Lyubchenko S and Dresselhaus M S 2003 *Appl. Phys. Lett.* **82** 2628
- [8] de Sande J C G, Missana T and Afonso C N 1996 *J. Appl. Phys.* **80** 7023
- [9] Boffoué M O, Lenoir B, Scherrer H and Dauscher A 1998 *Thin Solid Films* **322** 132

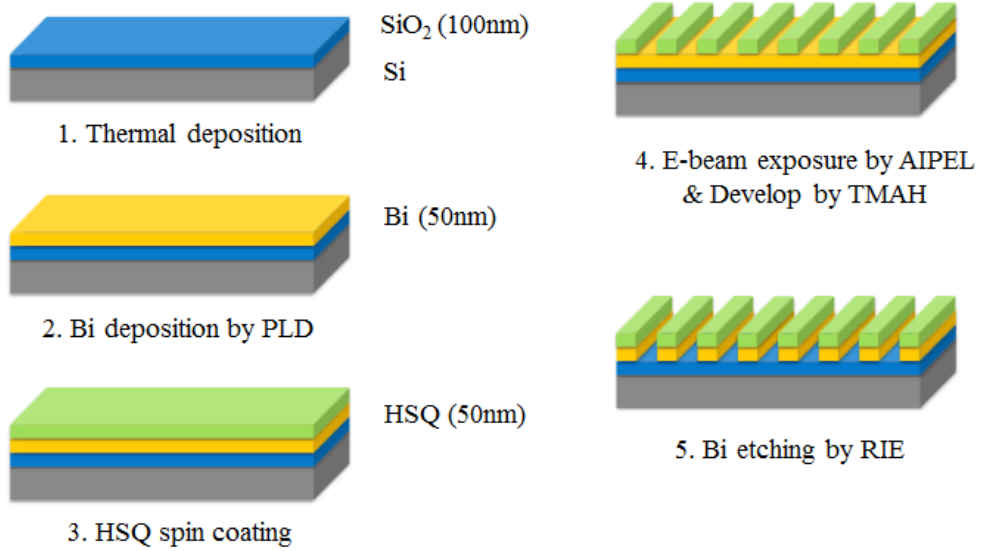
## CHAPTER 4.

### **Bismuth nanowire**

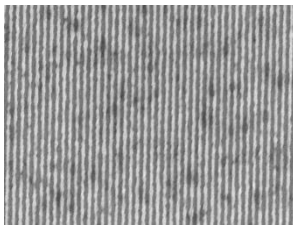
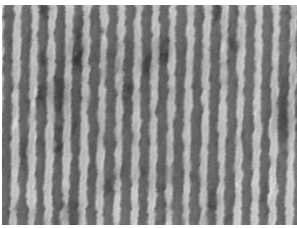
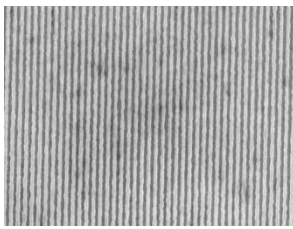
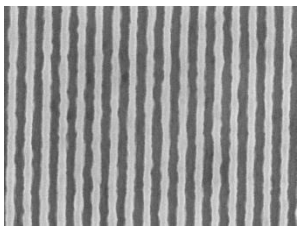
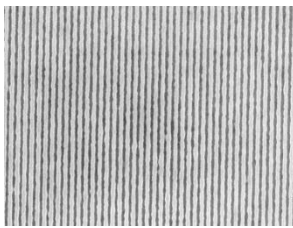
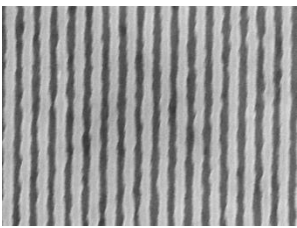
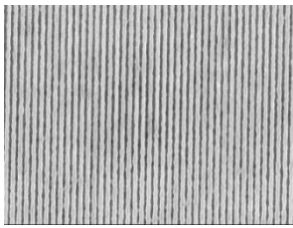
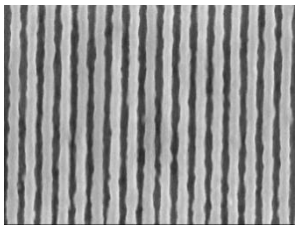
## 4.1. Experiments

The bismuth nanowires are fabricated by e-beam lithography process. The diagram of fabrication step is indicated in figure 4-8. First the SiO<sub>2</sub> was deposited by thermal deposition with the thickness of 100nm. The main reason of depositing SiO<sub>2</sub> layer is electrically insulating between bismuth layer and Si substrate. Then bismuth thin-film (thickness: 50nm) was deposited by pulsed laser deposition (PLD) system with optimized condition for bismuth thin-film which has fine surface and high electrical conductivity. And hydrogen silsesquioxane (HSQ) was spin coated on the bismuth thin-film as an e-beam resist. Then electron beam was exposed on the coated HSQ with various e-beam dose ( 850 ~ 1000  $\mu\text{C}/\text{cm}^2$  ). The line pattern was developed with tetramethylammonium hydroxide (TMAH) solution for 1min at room temperature. Then the sample was located in the reactive ion etch chamber (Oxford, RIE 80 plus) and dry etched with BCl<sub>3</sub> and Cl<sub>2</sub> based recipe to develop bismuth nanowire. After bismuth nanowire was defined, the temperature dependent electrical property was measured with Au electrodes. The Au electrodes were fabricated by lift-off process. First, photo resist (AZ5214) was spin coated on the bismuth nanowire sample and the electrodes pattern was developed, then the Au

thin-film (50nm thickness) was deposited by e-beam evaporator on the sample and Au electrodes were defined by removing the photo resist by acetone. The temperature dependent electrical property of bismuth thin-film was measured by 4-point-probe method and temperature dependent electrical property of bulk bismuth and bismuth nanowire was measured by 2-point contact method. The electrical resistances of the samples were measured with parameter analyzer (Agilent, 4156C). Then the electrical resistivity was obtained with their dimensions, respectively.



**Figure 4-1. Schematic diagram of bismuth nanowire fabrication step**

Dose ( $\mu\text{C}/\text{cm}^2$ )	SEM images		Width of nanowire
850			~55nm
900			~60nm
950			~70nm
1000			~80nm

**Figure 4-2. SEM images of bismuth nanowire fabricated by e-beam lithography process.**

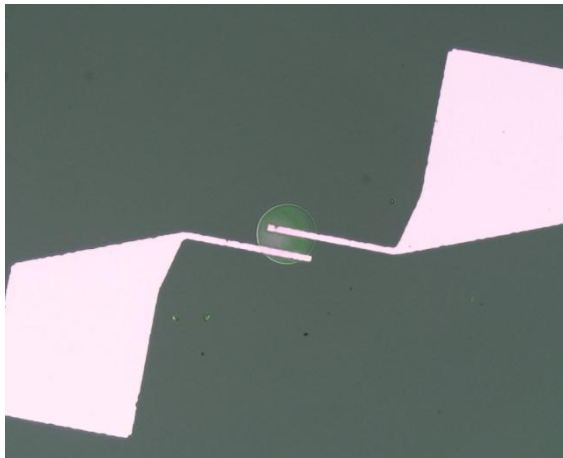


**Figure 4-3. Optic image of electrodes deposited on bismuth nanowire.**

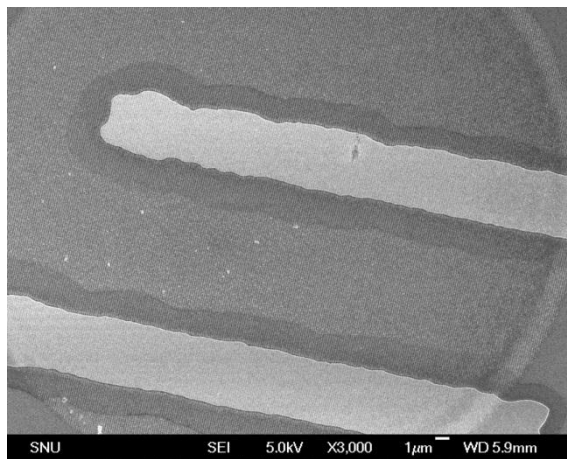


**Figure 4-4. SEM image of electrodes deposited on bismuth nanowire**



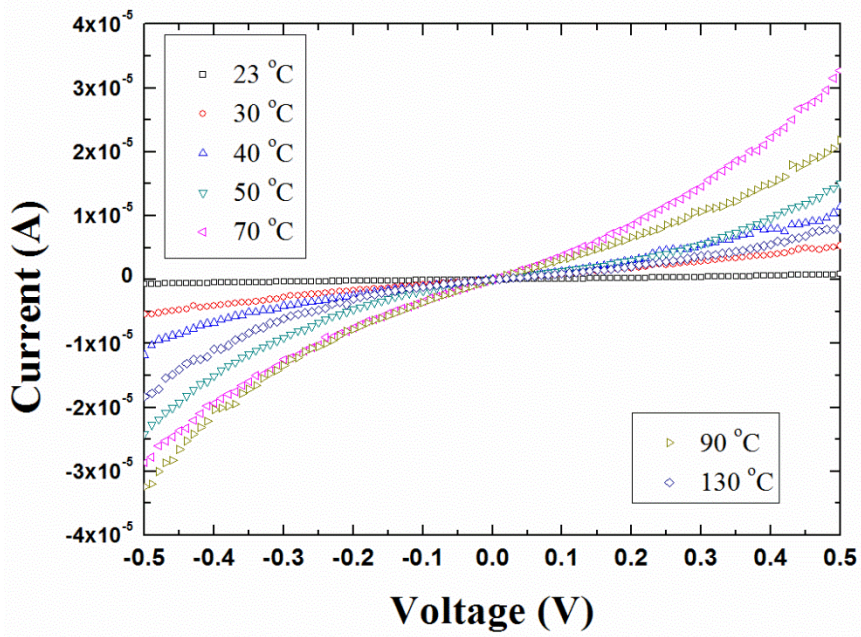


**Figure 4-5. Electrical property measurement of bismuth nanowire in various temperatures.**

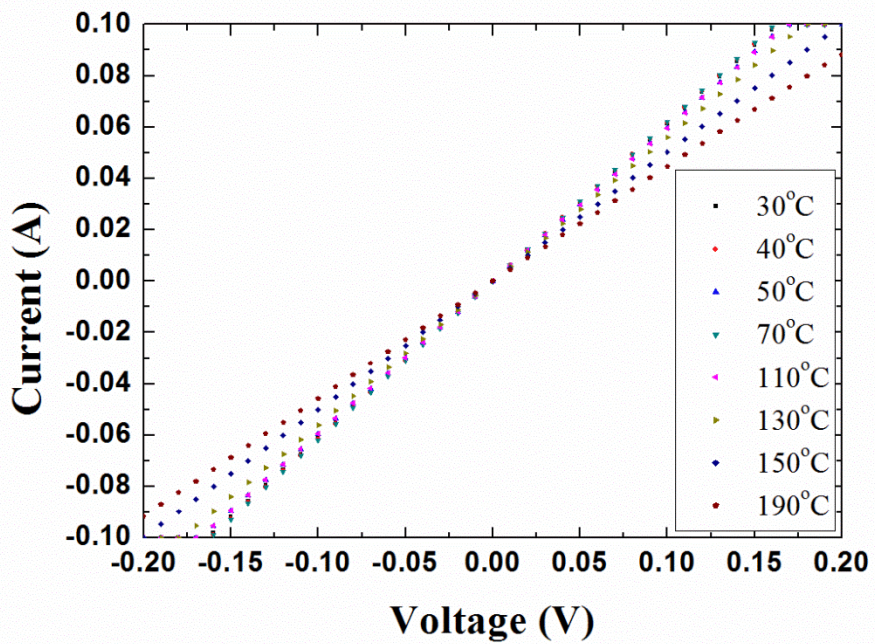


**Figure 4-6. Electrical property measurement of bulk bismuth in various temperatures.**

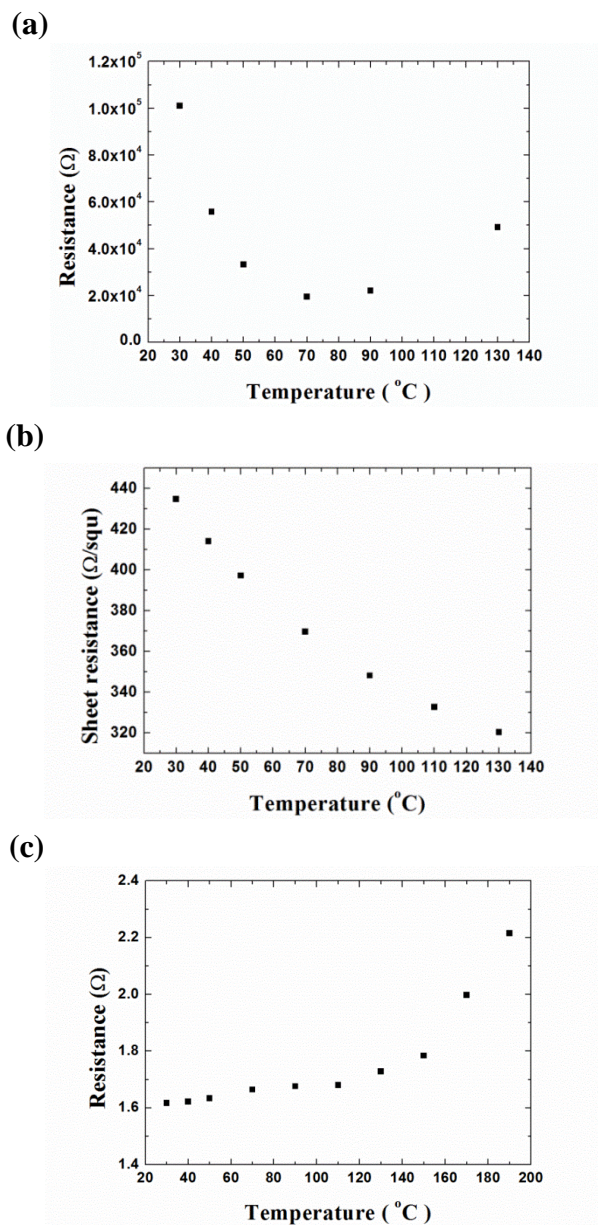


**Figure 4-7. Temperature dependent electrical resistance of bismuth nanowire (a), bismuth thin film (b), bulk bismuth (c).**

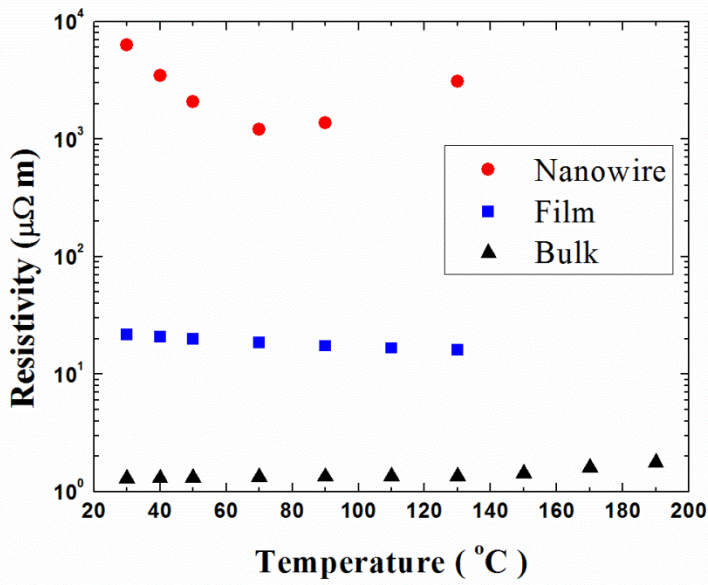


**Figure 4-8. Temperature dependent electrical resistivity of bismuth nanowire, thin film and bulk.**

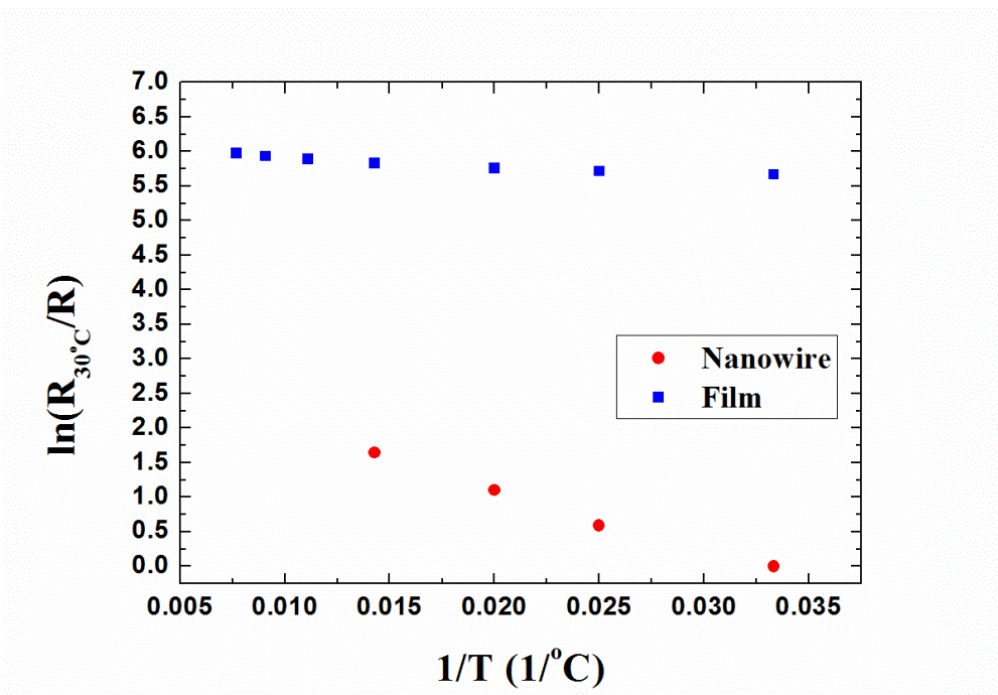


**Figure 4-9. Temperature dependent electrical resistivity of bismuth nanowire and thin film.**

## 4.2. Result and discussion

Figure 4-5 shows the voltage-sweep-curve of bismuth nanowire (70nm width) in various temperatures. Based on this curve, temperature dependent electrical resistance of bismuth nanowire was calculated and indicated in figure 4-7 (a). Figure 4-6 shows the voltage-sweep-curve of bulk bismuth (approximately,  $1\text{cm}^3$  hexahedron) in various temperatures. Based on this data, temperature dependent electrical resistance of bulk bismuth was calculated and indicated in figure 4-7 (c). Figure 4-7 (b) shows the temperature dependent sheet resistance of bismuth thin-film (50nm thickness). In the figure 4-7 (a), temperature dependent electrical resistance of bismuth nanowire has saturation point around  $70\text{ }^\circ\text{C}$ , and bismuth nanowire behaves like semiconducting materials. In the figure 4-7 (b), temperature dependent electrical resistance of bismuth thin-film is indicated and sheet resistance is decreasing as temperature increases in the experiment range. In the figure 4-7 (c), temperature dependent electrical resistance of bulk bismuth is indicated and the electrical resistance is increasing as temperature increases. In the figure 4-8, the electrical resistivity of bulk bismuth and bismuth thin film and bismuth nanowire is indicated. This graph was calculated from figure 4-7 and the dimensions of bulk bismuth, bismuth thin film

and bismuth nanowire. The temperature coefficient of resistivity (TCR) value of bulk bismuth is positive value ( $39e^{-4}$ ) and it is well matched with reference value ( $42e^{-4}$ ). In the figure 4-9, natural log plot of temperature dependent electrical resistivity is provided and the slopes in the graph indicate the thermal activation energy of bismuth thin film and bismuth nanowire. The thermal activation energy of bismuth thin film is 2.041meV and thermal activation energy of bismuth nanowire is 14.965meV. The thermal activation energy was increased by 7times in bismuth nanowire and it is believed that the increased activation energy was caused from increased scattering from surface and phonon in bismuth nanowire.

## Abstract (in Korean)

본 논문에서는 나노스케일의 공정기술이 열전소자에 사용되는 재료에 적용되었을 때 열전성능과 전기적 성능을 밝혀보고자 하였다. 나노스케일의 공정기술이 열전성능을 높일 수 있다는 가능성이 발표된 후 나노메쉬 (Nanomesh) 구조와 나노와이어 (Nanowire) 구조가 잠재적으로 열전소자에 쓰일 수 있는 재료들에 적용이 되었다. 본 논문에서는 나노메쉬와 나노와이어 구조가 각각 CNT film과 bismuth에 적용을 시켜 전기적, 열적 transport 특성에 관하여 분석한 결과를 고찰하였다. 첫 번째로, 나노메쉬 패턴을 CNT film에 삽입한 nanomesh CNT film과 나노메쉬 패턴을 삽입하지 않은 pristine CNT film의 전기적, 열적 광학적 특성을 비교하였다. Metallic carbon nanotube는 Seebeck coefficient가 0에 가까워야 함에도 불구하고 nanotube film은 상당히 높은 Seebeck coefficient를 가지고 있다. 본 실험에서는 anodized aluminum oxide membrane을 etching hard mask로 이용하여 nanomesh pattern을 CNT film에 삽입하였다. 조밀한 나노스케일의 hole들이 patterning 되어 삽입된 CNT film의 thermoelectric power가 30%



(29 to 39 V/K) 가량 증가된 것이 관찰되었다. 이러한 현상을 Nano-patterning에 의한 electron localization 에 의한 것으로 설명하였다. 두 번째로, 표면의 거칠기가 낮은 bismuth film을 증착하기 위해 pulsed laser deposition (PLD) system의 증착조건이 최적화 되었다. Bismuth film의 전기적 특성과 표면의 거칠기를 PLD system의 Working pressure와 target to substrate (TS) distance, 그리고 기판의 온도를 조절해 가며 관찰 하였다. 각 증착 parameter 들의 영역은 working pressure의 경우 10 mTorr 에서 base pressure (10<sup>-6</sup> Torr), TS distance의 경우 4cm ~ 7cm, 그리고 기판의 온도는 22 °C 에서 200 °C까지 조절하였다. Bismuth film의 electrical resistivity와 표면의 거칠기는 working pressure, TS distance, 그리고 기판의 온도에 따라 달라지는 경향을 보였으며, 최적화 된 조건에서 증착 된 bismuth film의 RMS surface roughness value는 1.57nm 이고 electrical resistivity는 300 $\mu\Omega$ cm 이다. 이러한 좋은 표면을 가진 필름을 바탕으로 하여 최종적으로 bismuth nanowire를 top-down fabrication 방식인 e-beam lithography를 통해 제작하였고 bismuth nanowire의 온도에 따른 전기적 성질을 bismuth thin film과 bulk bismuth와 비교해 보았다.

주요어: 열전, 나노메쉬 (nanomesh), AAO membrane,  
지백지수, CNT film, 비스무스 필름, 비스무스 hillock, Pulsed  
laser deposition

학번: 2010-22770